

Optical manipulation of bipolarons in a system with nonlinear electron-phonon coupling

K. Kovač,¹ D. Golež,^{1,2} M. Mierzejewski,³ and J. Bonča^{1,2}

¹*J. Stefan Institute, 1000 Ljubljana, Slovenia*

²*Faculty of Mathematics and Physics, University of Ljubljana, 1000 Ljubljana, Slovenia*

³*Department of Theoretical Physics, Faculty of Fundamental Problems of Technology, Wrocław University of Science and Technology, 50-370 Wrocław, Poland*

(Dated: January 31, 2024)

We investigate full quantum mechanical evolution of two electrons nonlinearly coupled to quantum phonons and simulate the dynamical response of the system subject to a short spatially uniform optical pulse that couples to dipole-active vibrational modes. Nonlinear electron-phonon coupling can either soften or stiffen the phonon frequency in the presence of electron density. In the former case, an external optical pulse tuned just below the phonon frequency generates attraction between electrons and leads to a long-lived bound state even after the optical pulse is switched off. It originates from a dynamical modification of the self-trapping potential that induces a metastable state. By increasing the pulse frequency, the attractive electron-electron interaction changes to repulsive. Two sequential optical pulses with different frequencies can switch between attractive and repulsive interaction. Finally, we show that the pulse-induced binding of electrons is shown to be efficient also for weakly dispersive optical phonons, in the presence anharmonic phonon spectrum and in two dimensions.

Research in the field of driven quantum materials is at the forefront of modern solid-state physics. The development of new laser sources opened a new chapter in the field¹ where we can selectively excite collective degrees of freedom, like lattice, magnetic and electronic excitations, to generate new emergent states of matter²⁻⁴. Among the most prominent examples are optical manipulation of magnetic order⁵⁻⁸, light-induced non-equilibrium metal-insulator transitions⁹⁻¹³, and optically enhanced transient states displaying superconducting signatures^{2,14-23}.

Modifying superconducting transition temperature by external stimulus was first shown using microwave radiation, now known as the Wyatt-Dayem effect²⁴⁻²⁶. More recently, it has been suggested that the selective excitation of a system could dramatically enhance the effect on the electronic system with nonlinear lattice couplings. A classic example includes a nonlinear coupling between optically excited infrared active mode inducing a Raman mode distortion^{12,27-29} with modified electronic properties. The idea was applied to cuprate superconductors³⁰, metal-insulator transition in manganites^{9,31} and paraelectric-ferroelectric transition in SrTiO₃^{32,33}. An even more interesting class of scenarios explores the role of quantum mechanical fluctuations on pairing from nonlinear phononics³⁴. We expect nonlinear electron-phonon coupling in crystals where light ions are symmetrically intercalated between heavy ions³⁵ like in organic crystals TMTSF₂-PF₆³⁶ or TTF-TCNQ^{37,38}. Recent experimental realization of strong nonlinear electron-phonon coupling was reported in one dimensional ET-F₂TCNQ and identified by the presence of strong second harmonics^{39,40}. In equilibrium, the nonlinear electron-phonon (EP) coupling leads to light polarons³⁵ and even more significantly to strongly bound light bipolarons⁴¹. Out of equilibrium, the squeezed electronic states due to nonlinear electron-lattice coupling can induce attraction between charge carriers inducing either superconducting⁴² or insulator-metal transition^{43,44}. The second class of ideas is based on the parametric resonance effect, where the interplay of driving and lattice non-linearities leads to enhanced electron-phonon interaction and pairing¹⁸. However, other studies point out the

competition between pairing, heating or phonon-induced disorder and, depending on the approximation employed, one or another could prevail^{45,46}. Therefore, obtaining exact results for a driven system to understand the competition and gauge which approximations are appropriate for these highly excited correlated states would be highly valuable.

In this Letter, we provide an exact time evolution of a two-electron system coupled non-linearly to lattice distortions and driven by an external laser pulse, which homogeneously excites dipolar active lattice modes. We show that electronic binding can be dramatically enhanced or reduced depending on the pulse protocol. The electron binding (or repulsion) remains enhanced due to modified bipolaronic self-trapping leading to a long-lived (metastable) state even after the pulse has been switched off. We show that the binding takes place only for negative values of non-linear electron-lattice couplings (frequency softening), which is in contrast with previously applied approximation predicting a sign independent binding^{18,42,44,46}. Finally, we show that the metastable state slowly decays if Einstein phonons acquire a finite bandwidth, still, the binding remains elevated in comparison to its value before the application of the pulse.

The model under the consideration is given by

$$H_0 = -t_{\text{el}} \sum_{\langle i,j \rangle, s} (c_{i,s}^\dagger c_{j,s} + \text{H.c.}) + g_2 \sum_j \hat{n}_j (a_j^\dagger + a_j)^2 + \omega_0 \sum_j a_j^\dagger a_j + U \sum_j n_{i,\uparrow} n_{i,\downarrow}, \quad (1)$$

where $\langle i, j \rangle$ represents summation over nearest neighbors, $c_{j,s}^\dagger$ and a_j^\dagger are electron and phonon creation operators at site j and spin s , respectively, $\hat{n}_j = \sum_s c_{j,s}^\dagger c_{j,s}$ represents the electron density operator, t_{el} the nearest-neighbor electron hopping amplitude, and ω_0 denotes the Einstein phonon frequency. From here and on we set $t_{\text{el}} = 1$. The second term in Eq. (1) represents a quadratic EP coupling, see the Supplemental information (SM)⁵³ for physical realizations, and the last term the on-site Coulomb repulsion.

Since the studied Hamiltonian exists in infinitely dimensional Hilbert space one needs to single out a subspace that is relevant for the studied problem. Here, we focus on the dynamics of electrons thus the relevant subspace contains states where multiple phononic excitations may exist in the close proximity of electrons. More distant (in real space) phonon excitations are discarded since they do not influence the distribution of electrons. In order to construct such subspace we have used a numerical method described in detail in Refs.^{47–52} as well as in the SM.⁵³ The method contains a single parameter N_h that determines the maximal distance between electrons as well as the maximal number of phonon excitations.

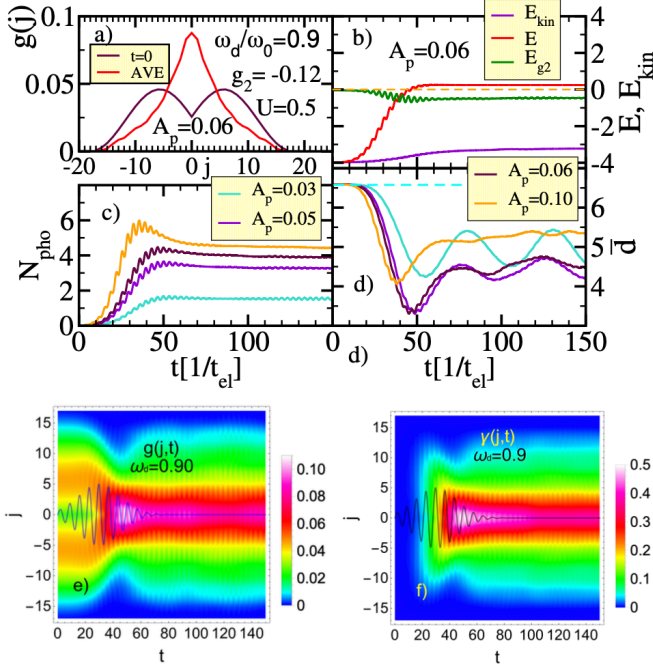


Figure 1: Different expectation values for 1D system: a) the density–density correlation function in the ground state $g(j, t = 0)$ and time–averaged $\bar{g}(j)$ in the time interval [45–150] after the pulse $V(t)$ with amplitude $A_p = 0.06$, $\sigma = 15$, $t_0 = 30$, and frequency $\omega_d/\omega_0 = 0.9$; b) the total energy $E(t) = \langle H \rangle_t$, the kinetic energy $E_{\text{kin}}(t) = \langle H_{\text{kin}} \rangle_t$ and EP coupling energy $E_{g_2}(t) = \langle H_{g_2} \rangle_t$ where H_{kin} and H_{g_2} represent the first and the second term in Eq. (1), respectively; c) the total number of phonon excitations $N_{\text{pho}} = \langle \sum_j a_j^\dagger a_j \rangle_t$ at different pulse amplitudes A_p ; d) the average particle distance \bar{d} ; e) the density–density correlation function $g(j, t)$; f) the number of phonons as a function of the inter–electron distance $\gamma(j, t)$; in e) and f) we used $A_p = 0.06$ and the shape of the pulse $V(t)$ is depicted with a blue line, while its vertical scale is in arbitrary units. In all figures, the driving frequency is $\omega_d/\omega_0 = 0.9$ and the electron–phonon coupling is $g_2 = -0.12$.

In the first part we present results for the one–dimensional (1D) case. We excite the system by driving an infrared active mode $H(t) = H_0 + V(t) \sum_j (a_j^\dagger + a_j)$ with a classical uniform AC field $V(t) = A_p \sin(\omega_d t) \exp[-(t - t_0)^2/2\sigma^2]$ that couples uniformly to all lattice displacements and time–propagate the full problem using the standard Lanczos procedure⁵⁴. Our first observable is the time evolution of the density–density

operator

$$\hat{g}(j) = \sum_i \hat{n}_{i,\uparrow} \hat{n}_{i+j,\downarrow}; \quad g(j, t) = \langle \hat{g}(j) \rangle_t, \quad (2)$$

where we use the following notation $\langle \hat{A} \rangle_t = \langle \psi(t) | \hat{A} | \psi(t) \rangle$. In the case of two electrons with the opposite spins, the operator $\hat{g}(j)$ is a projector which singles out states for which the distance between both electrons equals j and the average distance between electrons can be obtained as $\bar{d}(t) = \sum_j |j| g(j, t)$.

In Fig. 1 a) we present $g(j, t = 0)$ in the initial ground state of the system using a small Coulomb repulsion $U = 0.5$ that overcomes a weak phonon–mediated attraction. Functional dependence of $g(j, t = 0)$ is consistent with two electrons at an average distance $\bar{d}(t = 0) \sim 6.5$ as also seen from Fig. 1 d). Switching on the pulse $V(t)$ with a characteristic frequency $\omega_d/\omega_0 = 0.9$ and different amplitudes A_p causes the increase of the total and kinetic energies, E and E_{kin} , respectively, and a slight decrease of EP coupling energy E_{g_2} , see Fig. 1 b). For definitions see the caption of Fig. 1. The increase of E is predominantly due to the increase of the total number of phonon quanta N_{pho} , shown in Fig. 1 c). The most notable effect of the pulse is a substantial decrease of the average distance \bar{d} between electrons, seen in Fig. 1 d). While the increase of N_{pho} with increasing A_p up to $A_p = 0.08$ is monotonous, the decrease of \bar{d} is not and the largest drop is achieved around $A_p \sim 0.06 \pm 0.02$. The non–monotonous behavior originates from the competition between the heating effects and the pairing⁴⁵. In Fig. 1 e) the time evolution of the $g(j, t)$ under the influence of the optical pulse is presented as a density plot conjointly with the time evolution of the pulse, $V(t)$. We observe a distinct increase of the double occupancy, given by $g(0, t)$ that peaks around $t \sim 40$. The increased double occupancy persists even long after the pulse has been switched off creating a very long–lived (metastable) state, which for the case of Einstein phonons persist almost undistorted up to the largest times used in our calculation. This is consistent also with a time–averaged $\bar{g}(j)$ as seen in Fig. 1 a) displaying a peak at $j = 0$ in a sharp contrast with its value in the ground state $g(j, 0)$. These observations are in a stark contrast to the Floquet–type scenario analyzed in Ref. 18, where the attractive interaction is induced only during the pulse and in the following we will show that it originates from photo–modified self–trapping.

Now, we will explore how the long–lived state emerges due to the substantial absorption of the total energy predominantly stored in the increased number of phonon excitations. It is thus worthwhile determining the distribution of the number of phonons as a function of the relative distance between the electrons j . It is measured via the time evolution of $\gamma(j, t) = \langle \hat{\gamma}(j) \rangle_t$ where

$$\hat{\gamma}(j) = \hat{g}(j) \sum_l a_l^\dagger a_l, \quad (3)$$

describes the total number of phonons in states where the distance between electrons equals j . As it is shown in Fig. 1 f), most of the excess phonon excitations are absorbed by doubly

occupied states, i.e. $j = 0$, and those where electrons are in close proximity. It seems as if the excess phonon excitations represent the *glue* that at least for the given driving frequency $\omega_d/\omega_0 = 0.9$ provides a self-trapped attractive potential.

Searching further for the origin of the optically induced electron-electron potential we realize that it can only originate from the non-linear electron-phonon interaction term in Eq. (1), i.e. from the term $H_{g2} = g_2 \sum_j \hat{n}_j (a_j^\dagger + a_j)^2$. We define an effective potential by projecting H_{g2} on a subspace with a specified distance between electrons:

$$\hat{v}(j) = \hat{g}(j)H_{g2}, \quad (4)$$

that yields the time evolution of the effective potential $v(j, t) = \langle \hat{v}(j) \rangle_t$. This definition is further justified by the sum-rule that gives the total interacting energy $\sum_j v(j, t) = E_{g2}(t)$ shown in Fig. 1 b).

Motivated by previous Floquet analysis¹⁸ and a driven atomic limit analysis, see SM⁵³, predicting attractive (repulsive) electronic interaction for driving below (above) lattice frequency, we present $v(j, t)$ for two distinct driving frequencies leading to attractive $\omega_d/\omega_0 = 0.9$ and repulsive $\omega_d/\omega_0 = 1.1$ interaction for $g_2 = -0.12$, see Figs. 2 a) and b). When $\omega_d/\omega_0 = 0.9$ the pulse generates a pronounced peak located at $j = 0$, signaling the attractive effective potential that is most negative for the doubly occupied site. This is also presented in Fig. 2 c) where we show time averaged $\bar{v}(j)$. In contrast, at $\omega_d/\omega_0 = 1.1$, two minima appear around $j \pm 10$ that are further apart than the shallow minima in the ground state at $t = 0$, most clearly observed in Fig. 2 c). This is consistent with repulsive interaction considering that our computations are performed on a finite-size system. In Fig. 2 d) we further investigate the dependence of the effective potential on ω_d . We present time-averaged $\bar{v}(j)$ computed using different driving frequencies ω_d . While the strongest attractive interaction is observed around $\omega_d/\omega_0 = 0.9$, with increasing ω_d the minimum at $j = 0$ splits into two separate minima, consistent with the onset of a repulsive interaction. Around $\omega_d/\omega_0 = 1.1$ the separation of the local minima reaches its largest value $|j| \sim 10$. With further increase of ω_d the depth of the local minima diminishes and merges with the background. The presence of the minima after the pulse is in a clear distinction with the Floquet analysis, where the response is present only during the pulse. The dynamics of $v(j)$ shows that this interaction originates from the dynamical modification of the trapping potential leading to a long-lived state.

To obtain a deeper insight into this phenomenon we compute the time-averaged $\bar{g}(j)$ and the time averaged $\bar{\gamma}(j)$ and perform a scan over ω_d at $g_2 = -0.12$, see Figs 3 a) and b), respectively. For $\omega_d/\omega_0 \lesssim 0.8$ and $\omega_d/\omega_0 \gtrsim 1.3$, $\bar{g}(j)$ resembles its value in the ground state before the pulse has been switched on. This is consistent with the lack of the absorbed energy from the pulse as seen in Fig. 3 b) where we observe only a tiny amount of excess phonon excitations in the same ω_d regime. Near $\omega_d/\omega_0 \sim 0.9$, $\bar{g}(j)$ shows a pronounced maximum due to an increased weight of doubly occupied states ($j = 0$) consistent with an attractive electron-electron interaction. With increasing ω_d the attractive nature of interactions switches towards a repulsive one as the maximum of

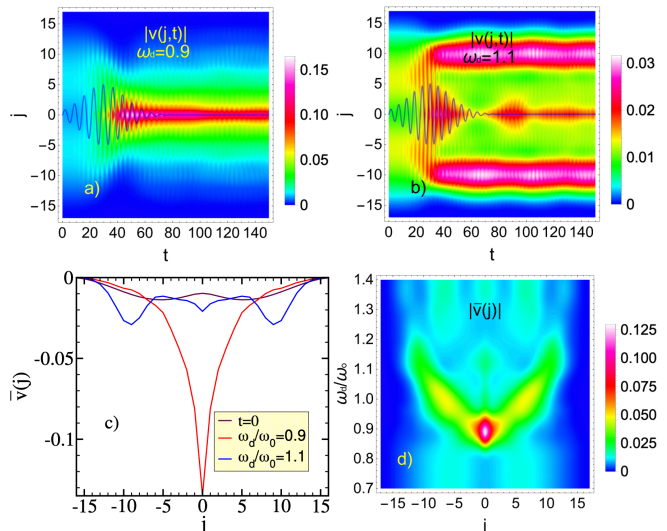


Figure 2: a) and b) magnitude of the effective potential $|v(j, t)|$ computed with two distinct driving frequencies $\omega_d/\omega_0 = 0.9$ and 1.1 , respectively. Note that the sign of $v(j, t)$ is strictly negative since $g_2 = -0.12$; c) the effective potential in the ground state, $v(j, 0)$, and time-averaged $\bar{v}(j)$ for two distinct ω_d . Time averages were performed in the same interval as in Fig. 1 a); d) time-averaged $\bar{v}(j)$ for different ω_d . We have used the pulse amplitude $A_p = 0.06$ while the other parameters are identical to those used in Fig. 1.

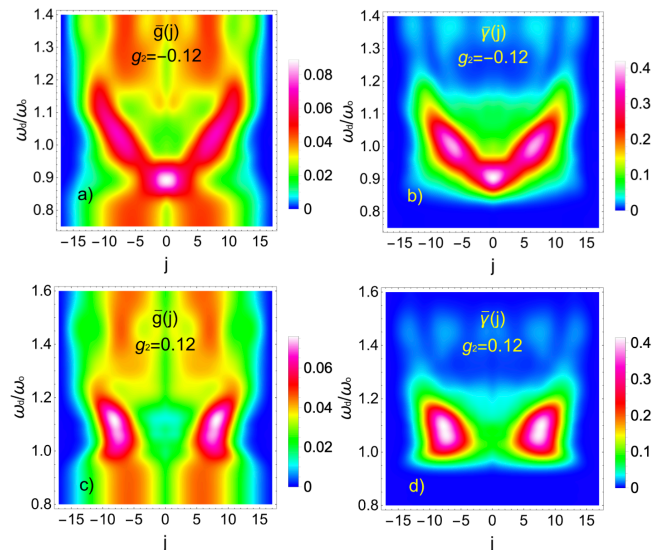


Figure 3: a) and c) the time-averaged density-density correlation function $\bar{g}(j)$ computed using different driving frequencies ω_d for $g_2 = -0.12$ and 0.12 , respectively; b) and d) time-averaged phonon distribution function $\bar{\gamma}(j)$. In all cases the time averages were performed in the same interval as in Figs. 1 a) and 2 d). We have used the pulse amplitude $A_p = 0.06$ while the rest of parameters are identical to those used in Fig. 1.

$\bar{g}(j)$ moves towards larger values of j . At $\omega_d/\omega_0 \sim 1.1$ the maximal value of $\bar{g}(j)$ appears around $j \sim \pm 10$ that exceeds its average value in the ground state signaling a strengthening

of the repulsive interaction.

The evolution of $\bar{g}(j)$ caused by changing driving frequencies ω_d is closely followed by the evolution of the absorbed phonon excitation distributions, $\bar{\gamma}(j)$, shown in Fig. 3 b). It is crucial to stress that time averages are performed in the regime where the optical pulse $V(t)$ that couples to all oscillators has been switched off. When the pulse is off-resonance, i.e. when $\omega_d/\omega_0 \gg 1$ or $\omega_d/\omega_0 \ll 1$, the system does not absorb much energy consequently, $\bar{\gamma}(j) \sim 0$ and $\bar{g}(j)$ remains close to its ground state value. It is worth pointing out that the maximum in the absorbed energy, presented in Fig. 3 b), appears at $\omega_d/\omega_0 \sim 0.96$ which is just above the value $\omega_d/\omega_0 \sim 0.9$ where maximal attractive interaction is observed. All this analysis shows that exactly at the resonance the heating effect dominates, but slightly below (above) the binding (repulsion) can win and remarkably leads to a very long-lived state due to the self-trapping mechanism. Remarkably, we observe that the self-trapping potential can be reversed by two successive optical pulses which can switch between attractive and repulsive electron-electron interactions, see SM⁵³.

In Figs. 3 c) and d) we show results for positive $g_2 = 0.12$. Absorption of energy from the pulse appears at higher ω_d than in the case when $g_2 < 0$, which is consistent with the increase of the phonon frequency in the presence of finite electron density for $g_2 > 0$. In contrast to $g_2 < 0$ case, the absorption of energy always leads to repulsive interaction. The observation contrasts with previous analysis^{18,42,44,46} based on the atomic limit or perturbative arguments, which predicted sign-independent pairing. Suppose this observation survives beyond the dilute limit. In that case, it poses a strong constraint on materials where we can expect light-induced long-lived attractive interaction due to the nonlinear electron-lattice couplings.

Now, we address how robust is the metastable state to various perturbations. In SM⁵³, we show the resilience to the presence of the linear EP coupling term, phonon dispersion, and anharmonic effects on the phonon spectrum. An important remaining question is whether the optically induced attraction survives in higher dimensions and we will demonstrate it for the two dimensional (2D) case of Eq. 1. The model can describe nonlinear coupling to phonon modes that are perpendicular to the plane. The system is defined on an infinite 2D plane, taking into account translational symmetry while the maximal distance between electrons is given by N_h and the maximal number of phonons in the system is $N_h - 1$ ^{47,48}.

Fig. 4a) shows the ground state density-density correlation function $g(x, y, t = 0)$, where $g(x, y, t) = \sum_{x', y'} \langle \hat{n}_{(x', y'), \uparrow} \hat{n}_{(x'+x, y'+y), \downarrow} \rangle_t$ at $g_2 = -0.12$. Due to the presence of nonzero $U = 0.5$ there is a shallow local minimum at the center, presenting the doubly occupied site; $x = y = 0$. Note also that $g(x, y, t)$ is normalized, i.e. $\sum_{x, y} g(x, y, t) = 1$, it therefore represents the probability for a state where the relative position of the electrons is given by (x, y) . In Fig. 4b) we present time-averaged $\bar{g}(x, y)$ after driving. The size of the bipolaron as a result of driving shrinks while the probability for double occupation increases. This is more quantitatively shown in Fig. 4c) where the average distance $\bar{d}(t)$ shows a substantial decrease during as

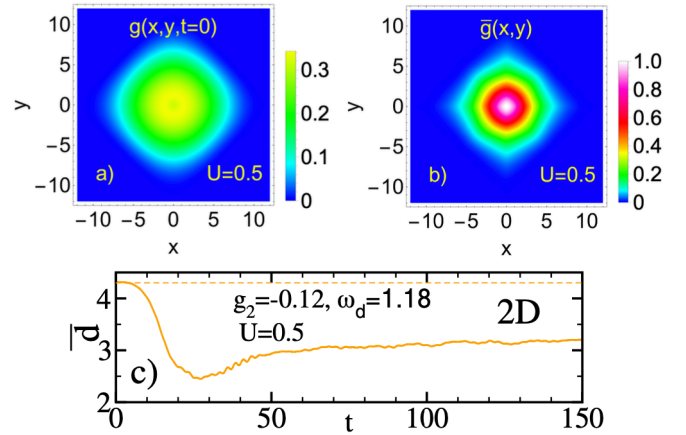


Figure 4: a) $g(x, y, t = 0)$ computed in the ground state at $\omega_0 = 1, g_2 = -0.12$ for the 2D version of the model in Eq. 1; b) time-averaged $\bar{g}(x, y)$ where time averages have been performed in the time interval $t \in [45, 150]$; to facilitate comparison between results computed before and after driving, we have rescaled the density plots so that the largest value of $\bar{g}(x, y)$ is set to unity; c) the average distance between particles $\bar{d}(t) = \sum_{x, y} \sqrt{x^2 + y^2} g(x, y, t)$. We have used $N_h = 12$ while the size of the Hilbert space was $N_{st}^{2D} \sim 2.6 \times 10^6$ and the rest of parameters of the model are the same as in the 1D case. For the driving field we have used the following parameters $\omega_d/\omega_0 = 1.18, A = 0.1, \sigma = 15, t_0 = 30$.

well as after the driving.

In conclusion, we have performed numerically exact time evolution of a bipolaron problem coupled by a non-linear electron-phonon interaction. When the electron-lattice interaction leads to phonon softening $g_2 < 0$, a properly tuned uniform optical pulse that couples to dipole-active lattice vibrations may optically induce either attractive or repulsive interaction between electrons. Here the primary mechanism originates from strong dependence of the effective phonon frequency on the local density of electrons⁴² so that an appropriately tuned pulse excites phonons corresponding to specific configurations of electrons. In 1D the strongest attractive interaction appears when pulses are tuned slightly below the Einstein phonon frequency ω_0 . This suggests that a softening of the lattice vibration due to an increased electron density and double occupancy plays an essential role in the appearance of the attractive potential between electrons. In contrast, a driving frequency slightly exceeding ω_0 generates repulsive interaction. In both cases, the effects of optically induced interactions persist long after the pulse has been switched off. Since the energy of the phonon subsystem depends on the density of electrons, both subsystems build an effective trap potential that mutually stabilizes the spatial configurations of electrons and phonons. We have demonstrated that optically induced interaction survives under various perturbations of the original Hamiltonian, such as: the introduction of weakly dispersive phonons, anharmonic effects on phonon frequency spectrum, and the introduction of the linear EP coupling. The mechanism is stable also in two and possibly also in higher dimensions. An important future problem is extending the bipolaron prob-

lem to finite doping to understand if we can induce coherence between these highly excited composite particles and to explore the experimental consequences of such states.

Acknowledgments

J.B., D.G. and K.K. acknowledge the support by the program No. P1-0044 and No. J1-2455 of the Slovenian Re-

search Agency (ARRS). J.B. acknowledge discussions with S.A. Trugman, A. Saxena and support from the Center for Integrated Nanotechnologies, a U.S. Department of Energy, Office of Basic Energy Sciences user facility and Physics of Condensed Matter and Complex Systems Group (T-4) at Los Alamos National Laboratory. M.M. acknowledges support by the National Science Centre, Poland via Project No. 2020/37/B/ST3/00020.

- ¹ D. N. Basov, R. D. Averitt, and D. Hsieh, *Nature Materials* **16**, 1077 (2017), URL <https://doi.org/10.1038/nmat5017>.
- ² C. Giannetti, M. Capone, D. Fausti, M. Fabrizio, F. Parmigiani, and D. Mihailovic, *Advances in Physics* **65**, 58 (2016), <https://doi.org/10.1080/00018732.2016.1194044>, URL <https://doi.org/10.1080/00018732.2016.1194044>.
- ³ P. Salén, M. Basini, S. Bonetti, J. Hebling, M. Krasilnikov, A. Y. Nikitin, G. Shamuilov, Z. Tibai, V. Zhaunerchyk, and V. Goryashko, *Physics Reports* **836-837**, 1 (2019), ISSN 0370-1573, matter manipulation with extreme terahertz light: Progress in the enabling THz technology, URL <https://www.sciencedirect.com/science/article/pii/S0370157319302649>.
- ⁴ A. de la Torre, D. M. Kennes, M. Claassen, S. Gerber, J. W. McIver, and M. A. Sentef, *Rev. Mod. Phys.* **93**, 041002 (2021), URL <https://link.aps.org/doi/10.1103/RevModPhys.93.041002>.
- ⁵ A. Kirilyuk, A. V. Kimel, and T. Rasing, *Rev. Mod. Phys.* **82**, 2731 (2010), URL <https://link.aps.org/doi/10.1103/RevModPhys.82.2731>.
- ⁶ M. Först, R. I. Tobey, S. Wall, H. Bromberger, V. Khanna, A. L. Cavalieri, Y.-D. Chuang, W. S. Lee, R. Moore, W. F. Schlotter, et al., *Phys. Rev. B* **84**, 241104 (2011), URL <https://link.aps.org/doi/10.1103/PhysRevB.84.241104>.
- ⁷ J. H. Mentink, K. Balzer, and M. Eckstein, *Nature Communications* **6**, 6708 (2015), URL <https://doi.org/10.1038/ncomms7708>.
- ⁸ T. F. Nova, A. Cartella, A. Cantaluppi, M. Först, D. Bossini, R. V. Mikhaylovskiy, A. V. Kimel, R. Merlin, and A. Cavalleri, *Nature Physics* **13**, 132 (2017), URL <https://doi.org/10.1038/nphys3925>.
- ⁹ M. Rini, R. Tobey, N. Dean, J. Itatani, Y. Tomioka, Y. Tokura, R. W. Schoenlein, and A. Cavalleri, *Nature* **449**, 72 (2007), URL <https://doi.org/10.1038/nature06119>.
- ¹⁰ H. Okamoto, H. Matsuzaki, T. Wakabayashi, Y. Takahashi, and T. Hasegawa, *Phys. Rev. Lett.* **98**, 037401 (2007), URL <https://link.aps.org/doi/10.1103/PhysRevLett.98.037401>.
- ¹¹ S. Kaiser, S. R. Clark, D. Nicoletti, G. Cotugno, R. I. Tobey, N. Dean, S. Lupi, H. Okamoto, T. Hasegawa, D. Jaksch, et al., *Scientific Reports* **4**, 3823 (2014), URL <https://doi.org/10.1038/srep03823>.
- ¹² A. Subedi, A. Cavalleri, and A. Georges, *Phys. Rev. B* **89**, 220301 (2014), URL <https://link.aps.org/doi/10.1103/PhysRevB.89.220301>.
- ¹³ L. Stojchevska, I. Vaskivskiy, T. Mertelj, P. Kusar, D. Svetin, S. Brazovskii, and D. Mihailovic, *Science* **344**, 177 (2014), <https://www.science.org/doi/pdf/10.1126/science.1241591>, URL <https://www.science.org/doi/abs/10.1126/science.1241591>.
- ¹⁴ D. Fausti, R. I. Tobey, N. Dean, S. Kaiser, A. Dienst, M. C. Hoffmann, S. Pyon, T. Takayama, H. Takagi, and A. Cavalleri, *Science* **331**, 189 (2011), <https://www.science.org/doi/pdf/10.1126/science.1197294>, URL <https://www.science.org/doi/abs/10.1126/science.1197294>.
- ¹⁵ W. Hu, S. Kaiser, D. Nicoletti, C. R. Hunt, I. Gierz, M. C. Hoffmann, M. Le Tacon, T. Loew, B. Keimer, and A. Cavalleri, *Nature Materials* **13**, 705 (2014), URL <https://doi.org/10.1038/nmat3963>.
- ¹⁶ M. Mitrano, A. Cantaluppi, D. Nicoletti, S. Kaiser, A. Perucchi, S. Lupi, P. Di Pietro, D. Pontiroli, M. Riccò, S. R. Clark, et al., *Nature* **530**, 461 (2016), URL <https://doi.org/10.1038/nature16522>.
- ¹⁷ M. Knap, M. Babadi, G. Refael, I. Martin, and E. Demler, *Phys. Rev. B* **94**, 214504 (2016), URL <https://link.aps.org/doi/10.1103/PhysRevB.94.214504>.
- ¹⁸ M. Babadi, M. Knap, I. Martin, G. Refael, and E. Demler, *Phys. Rev. B* **96**, 014512 (2017), URL <https://link.aps.org/doi/10.1103/PhysRevB.96.014512>.
- ¹⁹ A. F. Kemper, M. A. Sentef, B. Moritz, T. P. Devereaux, and J. K. Freericks, *Annalen der Physik* **529**, 1600235 (2017), <https://onlinelibrary.wiley.com/doi/pdf/10.1002/andp.201600235>, URL <https://onlinelibrary.wiley.com/doi/abs/10.1002/andp.201600235>.
- ²⁰ G. Mazza and A. Georges, *Phys. Rev. B* **96**, 064515 (2017), URL <https://link.aps.org/doi/10.1103/PhysRevB.96.064515>.
- ²¹ N. Bittner, T. Tohyama, S. Kaiser, and D. Manske, *Journal of the Physical Society of Japan* **88**, 044704 (2019), <https://doi.org/10.7566/JPSJ.88.044704>, URL <https://doi.org/10.7566/JPSJ.88.044704>.
- ²² A. Grankin, M. Hafezi, and V. M. Galitski, *Phys. Rev. B* **104**, L220503 (2021), URL <https://link.aps.org/doi/10.1103/PhysRevB.104.L220503>.
- ²³ M. Buzzi, D. Nicoletti, M. Fechner, N. Tancogne-Dejean, M. A. Sentef, A. Georges, T. Biesner, E. Uykur, M. Dressel, A. Henderson, et al., *Phys. Rev. X* **10**, 031028 (2020), URL <https://link.aps.org/doi/10.1103/PhysRevX.10.031028>.
- ²⁴ A. F. G. Wyatt, V. M. Dmitriev, W. S. Moore, and F. W. Sheard, *Phys. Rev. Lett.* **16**, 1166 (1966), URL <https://link.aps.org/doi/10.1103/PhysRevLett.16.1166>.
- ²⁵ A. H. Dayem and J. J. Wiegand, *Phys. Rev.* **155**, 419 (1967), URL <https://link.aps.org/doi/10.1103/PhysRev.155.419>.
- ²⁶ G. Eliashberg, *Tech. Rep., Inst. of Theoretical Physics, Moscow* (1970).

- ²⁷ M. Först, C. Manzoni, S. Kaiser, Y. Tomioka, Y. Tokura, R. Merlin, and A. Cavalleri, *Nature Physics* **7**, 854 (2011), URL <https://doi.org/10.1038/nphys2055>.
- ²⁸ A. S. Disa, T. F. Nova, and A. Cavalleri, *Nature Physics* **17**, 1087 (2021).
- ²⁹ A. Subedi, *Comptes Rendus. Physique* **22**, 161 (2021).
- ³⁰ R. Mankowsky, A. Subedi, M. Först, S. O. Mariager, M. Chollet, H. Lemke, J. S. Robinson, J. M. Glowina, M. P. Minitti, A. Frano, et al., *Nature* **516**, 71 (2014).
- ³¹ V. Esposito, M. Fechner, R. Mankowsky, H. Lemke, M. Chollet, J. M. Glowina, M. Nakamura, M. Kawasaki, Y. Tokura, U. Staub, et al., *Phys. Rev. Lett.* **118**, 247601 (2017), URL <https://link.aps.org/doi/10.1103/PhysRevLett.118.247601>.
- ³² A. Subedi, *Physical Review B* **95**, 134113 (2017).
- ³³ T. Nova, A. Disa, M. Fechner, and A. Cavalleri, *Science* **364**, 1075 (2019).
- ³⁴ D. E. Kiselov and M. V. Feigel'man, *Phys. Rev. B* **104**, L220506 (2021), URL <https://link.aps.org/doi/10.1103/PhysRevB.104.L220506>.
- ³⁵ C. P. J. Adolphs and M. Berciu, *Phys. Rev. B* **89**, 035122 (2014), URL <https://link.aps.org/doi/10.1103/PhysRevB.89.035122>.
- ³⁶ M. Kaveh, M. Weger, and L. Friedman, *Physical Review B* **26**, 3456 (1982).
- ³⁷ H. Gutfreund and M. Weger, *Physical Review B* **16**, 1753 (1977).
- ³⁸ O. Entin-Wohlman, H. Gutfreund, and M. Weger, *Journal of Physics C: Solid State Physics* **18**, L61 (1985).
- ³⁹ S. Kaiser, S. Clark, D. Nicoletti, G. Cotugno, R. Tobey, N. Dean, S. Lupi, H. Okamoto, T. Hasegawa, D. Jaksch, et al., *Scientific reports* **4**, 3823 (2014).
- ⁴⁰ R. Singla, G. Cotugno, S. Kaiser, M. Först, M. Mitrano, H. Liu, A. Cartella, C. Manzoni, H. Okamoto, T. Hasegawa, et al., *Physical Review Letters* **115**, 187401 (2015).
- ⁴¹ C. P. J. Adolphs and M. Berciu, *Phys. Rev. B* **90**, 085149 (2014), URL <https://link.aps.org/doi/10.1103/PhysRevB.90.085149>.
- ⁴² D. M. Kennes, E. Y. Wilner, D. R. Reichman, and A. J. Millis, *Nature Physics* **13**, 479 (2017), URL <https://doi.org/10.1038/nphys4024>.
- ⁴³ F. Grandi, J. Li, and M. Eckstein, *Phys. Rev. B* **103**, L041110 (2021), URL <https://link.aps.org/doi/10.1103/PhysRevB.103.L041110>.
- ⁴⁴ M. A. Sentef, *Phys. Rev. B* **95**, 205111 (2017), URL <https://link.aps.org/doi/10.1103/PhysRevB.95.205111>.
- ⁴⁵ Y. Murakami, N. Tsuji, M. Eckstein, and P. Werner, *Phys. Rev. B* **96**, 045125 (2017), URL <https://link.aps.org/doi/10.1103/PhysRevB.96.045125>.
- ⁴⁶ J. Sous, B. Kloss, D. M. Kennes, D. R. Reichman, and A. J. Millis, *Nature Communications* **12**, 5803 (2021), URL <https://doi.org/10.1038/s41467-021-26030-3>.
- ⁴⁷ J. Bonča, S. A. Trugman, and I. Batistić, *Phys. Rev. B* **60**, 1633 (1999).
- ⁴⁸ J. Bonča, T. K特拉šnik, and S. A. Trugman, *Phys. Rev. Lett.* **84**, 3153 (2000), URL <https://link.aps.org/doi/10.1103/PhysRevLett.84.3153>.
- ⁴⁹ L.-C. Ku, S. A. Trugman, and J. Bonča, *Phys. Rev. B* **65**, 174306 (2002), URL <https://link.aps.org/doi/10.1103/PhysRevB.65.174306>.
- ⁵⁰ D. Golež, J. Bonča, L. Vidmar, and S. A. Trugman, *Phys. Rev. Lett.* **109**, 236402 (2012), URL <https://link.aps.org/doi/10.1103/PhysRevLett.109.236402>.
- ⁵¹ J. Kogoj, M. Mierzejewski, and J. Bonča, *Phys. Rev. Lett.* **117**, 227002 (2016), URL <https://link.aps.org/doi/10.1103/PhysRevLett.117.227002>.
- ⁵² J. Bonča and S. A. Trugman, *Phys. Rev. B* **103**, 054304 (2021), URL <https://link.aps.org/doi/10.1103/PhysRevB.103.054304>.
- ⁵³ *See the supplemental material at [url will be inserted by publisher] for the description of the numerical method, resilience of the metastable state to various perturbations, results obtained with the driving frequency $\omega_d/\omega_0 = 1.1$, the response of the system for $g_2 = 0.5$, the finite hilbert-space analysis, the double pulse time evolution, the evolution of $g(j)$ with u , and analytic solution of the driven single-site problem.*
- ⁵⁴ P. T. Jun and J. C. Light, *J. Chem. Phys.* **85**, 5870 (1986).

Optical manipulation of bipolarons in a system with nonlinear electron-phonon coupling

K. Kovač,^{1,2} D. Golež,^{1,2} M. Mierzejewski,³ and J. Bonča^{1,2}

¹*J. Stefan Institute, 1000 Ljubljana, Slovenia*

²*Faculty of Mathematics and Physics, University of Ljubljana, 1000 Ljubljana, Slovenia*

³*Department of Theoretical Physics, Faculty of Fundamental Problems of Technology, Wrocław University of Science and Technology, 50-370 Wrocław, Poland*

I. NUMERICAL METHOD

The method is based on a construction of basis states for the many-body Hilbert space that can be written as $|j_1, j_2; \dots, n_m, n_{m+1}, \dots\rangle$, where the spin up and down electrons are on sites j_1 and j_2 , and there are n_m phonons on site m . A functional subspace is constructed iteratively beginning with an initial state where both electrons are on the same site with no phonons and applying the sum of operators $H_{\text{el}} + H_{\text{EP}}$ ($H_{\text{el}} = \sum_{j,s} (c_{j,s}^\dagger c_{j+1,s} + \text{H.c.})$) and $H_{\text{EP}} = \sum_j \hat{n}_j (a_j^\dagger + a_j)$) N_h times taking into account the full translational symmetry. The constructed Hilbert space defined on the one-dimensional chain allows only a finite maximal distance of a phonon quanta from the doubly occupied site, $L_{\text{max}_1} = (N_h - 1)/2$, a maximal distance between two electrons $L_{\text{max}_2} = N_h$, and a maximal amount of phonon quanta at the doubly occupied site $N_{\text{phmax}} = N_h$. The number of generation N_h is therefore our convergence parameter and by converging in it one can consider the solution numerically exact. The number of states in the many-body Hilbert space N_{st} in the 1D case increases with N_h exponentially as $N_{\text{st}}^{1\text{D}} \sim 6.4 \times 2^{1.02N_h}$ and in the 2D case as: $N_{\text{st}}^{2\text{D}} \sim 3.6 \times 3^{1.02N_h}$. Note that in the limit of large N_h the two respective Hilbert spaces would grow as $N_{\text{st}}^{1\text{D}} \sim 2^{N_h}$ and $N_{\text{st}}^{2\text{D}} \sim 3^{N_h}$.

II. INVARIABILITY OF OPTICALLY INDUCED INTERACTION AGAINST DIFFERENT PERTURBATIONS

A. Linear electron-phonon coupling term

We next demonstrate that the optically induced attraction survives also in the presence of the linear EP coupling, nevertheless, it does not occur without the presence of an anharmonic interaction. To this end, we test the influence of a linear EP coupling term $H_1 = g_1 \sum_j \hat{n}_j (a_j^\dagger + a_j)$ on the dynamic response of H_0 as studied in the main text. In Fig. 1 we show results obtained after the time propagation with the Hamiltonian $\tilde{H}(t) = H_0 + H_1 + V(t) \sum_j (a_j^\dagger + a_j)$. In Fig. 1 a) we first present time-averaged $\bar{g}(j)$ obtained using different ω_d at $g_2 = -0.12$ and $g_1 = 0.1$. We compare results obtained at finite g_1 to those when $g_1 = 0.0$, as shown in Fig. 3 a) of the main text. Close to $\omega_d = 0.9$ we observe an attractive electron-electron interaction that crosses over to repulsive with increasing ω_d , nevertheless, the crossover is not as pronounced as in the $g_1 = 0$ case. A closer inspection of the time propagation at $\omega_d = 0.88$, as presented in Fig. 1 b), reveals

pronounced oscillations of the metastable bound state. This is in contrast with results for $g_1 = 0.0$, presented in Fig. 1 e) of the main text, where oscillations are much less pronounced.

We next set $g_2 = 0.0$ and by investigating results presented in Figs. 1 c), d), and e) we consider whether only the linear EP coupling term is sufficient to induce dynamically generated interaction between electrons. In comparison between Fig. 1 a), of SM and Fig. 3 a) of the main text, we do not observe a clear signal consistent with the optically induced attractive interaction, see also Fig. 1 d). Instead, around $\omega_d/\omega_0 = 1.04$, presented in Fig. 1 e), a signature of a repulsive interaction is found.

B. Significance of the anharmonic effects in the phonon spectrum.

In the main text we have considered the anharmonic EP coupling, however, for the sake of simplicity, the phonon spectra were assumed to be the same as in the case of a simple harmonic oscillator. Below, we demonstrate that our conclusions concerning the optically induced attraction hold true also beyond this simplification. To this end we first solve the eigenproblem for the anharmonic oscillator: $H_4 = \alpha[\omega_0 a^\dagger a + g_4 (a^\dagger + a)^4]$. In order to disentangle the anharmonic effects from a trivial shift of the first excited state, the energy spectrum of H_4 is renormalized by a constant α . The value of α is set by the condition $\epsilon_1 - \epsilon_0 = \omega_0$, where ϵ_0 and ϵ_1 are, respectively, the ground state and the first excited state energies of H_4 . Finally, we perform the time evolution of $H(t) = H_0 + V(t) \sum_j (a_j^\dagger + a_j)$, where the original phonon spectrum on each site: $0, \omega_0, 2\omega_0, 3\omega_0, \dots$ is replaced by the renormalized anharmonic spectrum of H_4 . For example, in the case when $\omega_0 = 1$ and $g_4 = 0.12$, the renormalized spectrum is given by: $0, \omega_0, 2.23\omega_0, 3.61\omega_0, \dots$. As observed in Figs. 2 a) and b), the dynamically induced electron-electron interaction remains robust upon the anharmonic modification of the phonon spectrum. At resonant driving frequency a metastable bound bipolaron is formed that consists of two electrons located predominantly on adjacent sites.

C. Dispersive phonons

We explore the long-lived stability of the optically driven attraction between electrons as seen in Fig. 1 e) in the main text, against the introduction of optical phonon dispersion. In Figs. 3 a) and b) we show $g(j, t)$ and $\gamma(j, t)$ obtained from a modified hamiltonian $H = H_0 -$

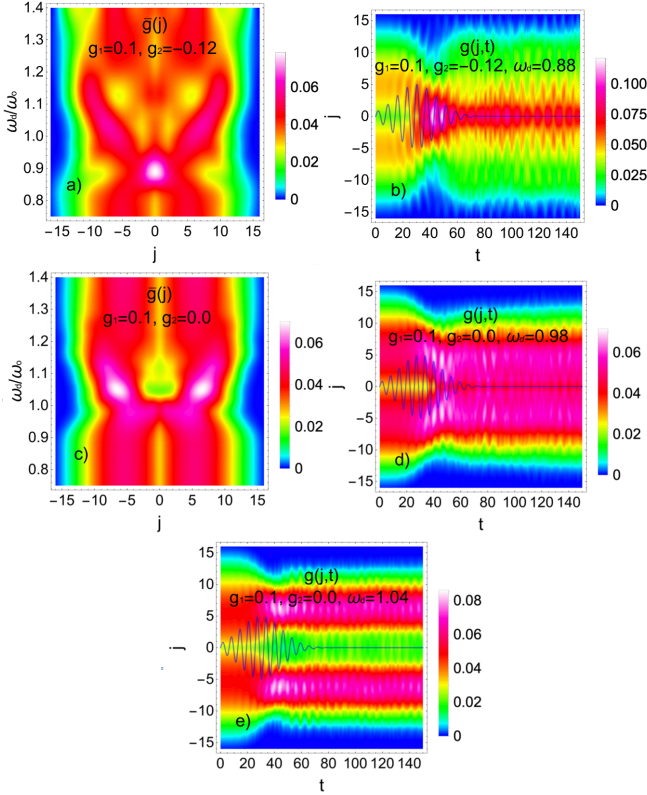


Figure 1: a) and c) the time-averaged density-density correlation function $\bar{g}(j)$ computed using different driving frequencies ω_d , linear coupling term $g_1 = 0.1$, and two different values of $g_2 = -0.12$ in a) and $g_2 = 0.0$ in c); in b), d), and e) we present the time evolutions of $g(j, t)$ for parameters, presented in a) and c) while choosing driving frequencies $\omega_d/\omega_0 = 0.88, 0.98$ and 1.04 where maximal attractive or repulsive interaction is expected. In a) and c) the time averages were performed in the same interval as in Fig. 1 of the main text. We have used the pulse amplitude $A_p = 0.06$, $U = 0.5$, and $N_h = 16$.

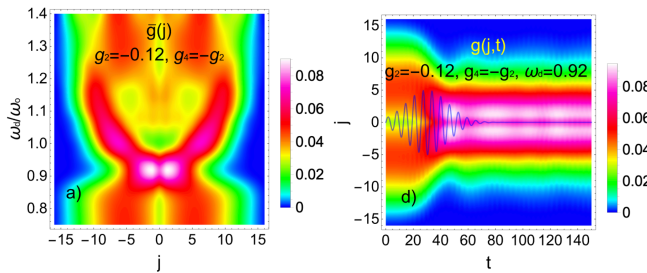


Figure 2: a) the time-averaged density-density correlation function $\bar{g}(j)$ computed using different driving frequencies ω_d , and a renormalized anharmonic phonon spectrum computed at $g_4 = 0.12$; in b) we present the time evolutions of $g(j, t)$ at driving frequency $\omega_d/\omega_0 = 0.92$. In all cases the time averages were performed in the same interval as in Fig. 1 of the main text. We have used the pulse amplitude $A_p = 0.06$, $U = 0.5$, and $N_h = 16$.

$W_{\text{ph}}/4 \sum_j (a_j^\dagger a_{j+1} + H.c.)$. The second term introduces dispersion among optical phonons with the bandwidth W_{ph} .

While the initial decrease of \bar{d} during the pulse, shown in Fig. 3 c), is comparable to $W_{\text{ph}} = 0$ case, we observe a slow relaxation towards $\bar{d}_\infty < \bar{d}_0$ with a relaxation time $\tau_{\bar{d}} \sim 50 \gg 1/W_{\text{ph}}$ as the pulse is switched off. In contrast, the double occupancy $D_t = \langle \hat{n}_\uparrow \hat{n}_\downarrow \rangle_t$, presented in Fig. 3 d), shows a larger increase at finite W_{ph} during the pulse, followed by a slow decrease with a relaxation time $\tau_D \sim \tau_{\bar{d}}$ towards $D_\infty > D_0$ where D_0 and \bar{d}_0 represent their respective values in the equilibrium. Even though the introduction of finite W_{ph} results in the initial decrease of $D(t)$ after the pulse, the value of D_∞ is consistent with the attractive interaction surviving the introduction of W_{ph} .

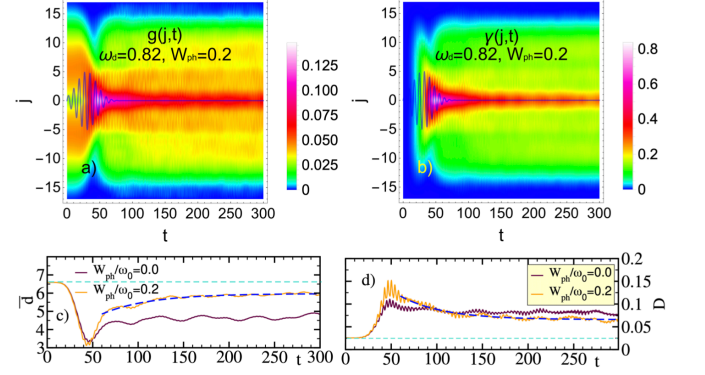


Figure 3: Correlation a) $g(j, t)$ and b) $\gamma(j, t)$ for dispersive optical phonons using $W_{\text{ph}} = 0.2$ and optimal driving frequency $\omega_d/\omega_0 = 0.82$ that at chosen W_{ph} yields maximal attractive interaction; c) and d) present comparison of $\bar{d}(t)$ and $N_{\text{pho}}(t)$, respectively. Exponential fits (blue dashed lines) in c) and d), of the form $A(t) = A \exp(-t/\tau) + A_\infty$, yield $(\tau_{\bar{d}}, \bar{d}_\infty) \sim (53, 6.0)$ and $(\tau_D, D_\infty) \sim (48, 0.07)$, respectively. The other parameters are identical to those used in Figs. 1 e) and f) in the main text.

D. Next-nearest-neighbor electron hopping

We explore the influence of the next-nearest-neighbour electron hopping term. The modified Hamiltonian is given by: $H = H_0 + t_2 \sum_{i,s} (c_{i,s}^\dagger c_{i+2,s} + H.c.)$, results are presented in Fig. 4. The addition of next-nearest-neighbour hopping brings about only small changes to the optically generated interaction between electrons. There is a visible shift in the optimal driving frequency of the optical pulse ω_d that generates strongest attractive interaction. In addition, a positive value of $t_2 = 0.1$ slightly increases attractive interaction in the ground state, while the effect of $t_2 = -0.1$ is opposite, see Fig. 4c). This is best seen comparing different \bar{d} for $\omega_s/\omega_0 \lesssim 0.75$ that are nearly identical to those in the ground state since the system does not absorb energy in the low ω_d regime. The effect that t_2 has on the ground state properties is reflected also in the optically excited states since the time-averaged values of $\bar{g}(j)$ show smaller average distance between electrons for $t_2 > 0$ in comparison to its opposite sign. Results should also be compared with Fig. 3a) of the main text.

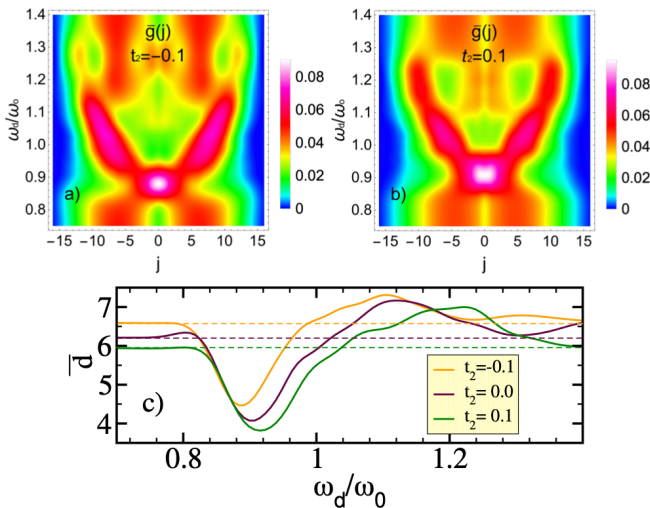


Figure 4: a) and b) $\bar{g}(j)$ using different values of $t_2 = -0.1$ and 0.1 , respectively; c) time-averaged average distance \bar{d} vs. the driving frequency for different values of t_2 . The rest of parameters, $\omega_0 = 1.0$, $g_2 = -0.12$, and $U = 0.5$, are identical to those used in Fig.3a) of the main text. Time averages were performed after the pulse has been switched off. Hilbert space was generated using $N_h = 16$.

III. DRIVING WITH $\omega_d/\omega_0 = 1.1$

In Fig. 5 we present the time evolution of $g(j, t)$ and $\gamma(j, t)$ under the influence of the optical pulse with the driving frequency $\omega_d/\omega_0 = 1.1$ that generates repulsive interaction between the electrons. In comparison to the case presented in Fig. 1e) of the main text where the central driving frequency is $\omega_d/\omega_0 = 0.9$, the maximum of $g(j, t)$ is around $j \sim 0$, in Fig. 5 a) the peak in $g(j, t)$ is around $j \sim 10$. In addition, the increase of $\gamma(j, t)$ is more evenly spread to $j \neq 0$ in Fig. 5 b) than in Fig. 1(f) of the main text .

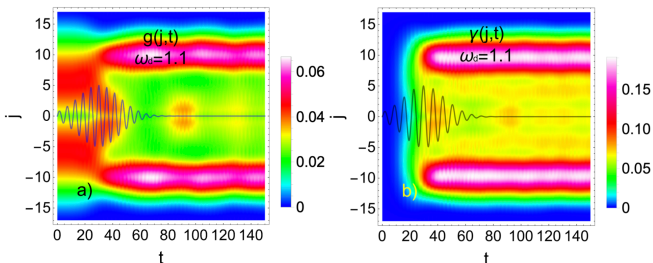


Figure 5: Time-dependent correlation functions at $\omega_d/\omega_0 = 1.1$. a) the density-density correlation function $g(j, t)$; b) the number of phonons as a function of the inter-electron distance $\gamma(j, t)$. In both cases the shape of the pulse $A(t)$ with $\omega_d/\omega_0 = 1.1$ is shown, its vertical scale is in arbitrary units. The rest of parameters is the same as used to generate Fig. 1(e) and (f).

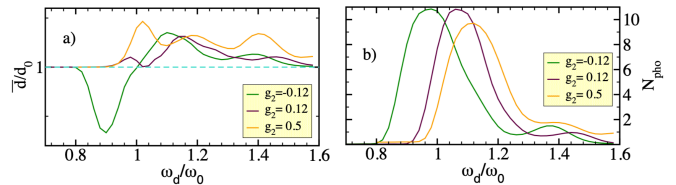


Figure 6: The time-averaged correlation functions computed at $g_2 = \pm 0.12$, and 0.5 for different driving frequencies ω_d . Time averages are defined as in Fig. 3 of the main text; a) represents the time-averaged distance relative to its ground state value d_0 , \bar{d}/d_0 and b) the total number of phonons N_{pho} . The rest of parameters are identical to those used in Fig. (3) of the main text.

IV. RESPONSE OF THE SYSTEM FOR $g_2 > 0$

In Fig. 6 we analyse the response of the system to different driving frequencies in the case of positive quadratic EP coupling $g_2 = 0.12$ and 0.5 . This analysis has been stimulated by the results presented in Ref.¹ where authors analyse the atomic limit of the model in Eq. (1). They compute the effective electron-electron interaction U^* of the model by comparing energies of zero, one and two electrons on the atomic site with an equal number of phonon excitations N_{pho} that gives:

$$U^* = U - (N_{\text{pho}} + \frac{1}{2})\omega_0 \left[2\sqrt{1 + 4g_2/\omega_0} - 1 - \sqrt{1 + 8g_2/\omega_0} \right]. \quad (1)$$

The second term in Eq. 1 is negative for any finite value of $g_2 > -\omega_0/8$, nevertheless, its value is asymmetric around $g_2 = 0$. For example, in the case of $g_2 = -0.12$, one obtains similar renormalization U^* as for $g_2 = 0.5$. This suggests an inquiry whether a positive g_2 that gives similar renormalization in the atomic limit also leads to attractive interaction when subject to an optical pulse with a well-tuned frequency.

In Fig. 6(a) and (b) we show time-averaged \bar{d} and N_{pho} as functions of ω_d for $g_2 = -0.12$ and two positive values $g_2 = 0.12$ and 0.5 . For $g_2 > 0$ \bar{d} always increases, consistent with the repulsive interaction, providing that ω_d is chosen such that the system absorbs energy from the pulse that leads to the increase of N_{pho} . When comparing results for $g_2 = -0.12$ and $+0.12$ we observe a very similar increase of N_{pho} with the only observable difference in the shift of the $g_2 = 0.12$ result towards slightly larger ω_d . In contrast, for $g_2 = -0.12$, \bar{d} is consistent with attractive interaction for $0.8 \lesssim \omega_d/\omega_0 \lesssim 1.0$ and repulsive for $1.0 \lesssim \omega_d/\omega_0 \lesssim 1.6$. It is worth stressing that in the latter case, the deep in \bar{d} is reached around $\omega_d/\omega_0 = 0.9$ while the peak in N_{pho} appears around $\omega_d/\omega_0 = 0.96$.

V. FINITE HILBERT SPACE ANALYSIS

In Fig. 7 we show how the time-averaged \bar{d} changes with increasing size of the Hilbert space N_{st}^{1D} as a function of ω_d . Note first that N_h that sets the number of many-body Hilbert states $N_{\text{st}}^{1D} \sim 6.4 \times 2^{1.02N_h}$ also defines the maximal allowed distance between electrons. The decrease of \bar{d}

around $\omega_d/\omega_0 \sim 0.9$ seems to be well converged in terms of the optimal value of ω_d that yields maximal drop of \bar{d} as well as its relative change \bar{d}/d_0 . In contrast, the increase of \bar{d}/d_0 that indicates repulsion at $\omega_d/\omega_0 > 1$ grows in size. This is consistent with the repulsive nature of interaction taking into account limited distance between the electrons due to the restricted Hilbert space. In the inset of the top panel of Fig. 7 we show d_0 in the ground state for different N_h . Even though the average distance d_0 before the application of the pulse increases with the system size due to finite $U = 0.5$, the relative decrease \bar{d}/d_0 seems to converge with increasing N_h signaling the effectiveness of the optically induced attractive interaction.

In Figs. 7a) through d) we show the evolution of time-averaged $\bar{g}(j)$ with the system size. It seems that by increasing the system size the switching between the attractive and repulsive interaction becomes even more pronounced.

VI. DOUBLE PULSE

In Fig. 8 we present a simulation of a system with $g_2 = -0.12$ subject to two consecutive optical pulses with different driving frequencies and amplitudes. The simulation starts from a ground state with $U = 0.5$ and the average distance between electrons $\bar{d} \sim 6.5$. A pulse with $\omega_{d1}/\omega_0 = 0.9$ is switched on that gives rise to an attractive interaction resulting in a decrease of \bar{d} as shown in Fig. 8 d) while $g(j, t)$ peaks around $j = 0$, as consistent with the increase of double occupancy. The second pulse with $\omega_{d2}/\omega_0 = 1.1$ results in the increase of \bar{d} indicating the change of the interaction from attractive to repulsive. Both pulses lead to an increase of the total as well as the kinetic energy, E and E_{kin} , respectively, as seen in Fig. 8 b) and a slight drop of the EP coupling energy E_{g2} .

VII. THE EVOLUTION OF $g(j)$ WITH U

In Figs. 9 a) and c) we first present the evolution of $g(j, t = 0)$ in the ground state with increasing U for $g_2 = -0.12$ and 0.12 , respectively. Even though the two plots seem identical, there are subtle differences since the Hamiltonian is not invariant to the sign change of g_2 . In Figs. 9 b) and d) we present $\bar{g}(j)$ vs. U , time-averaged after the driving pulse for the same values of g_2 as in a) and c). While $g_2 > 0$ tends to stabilise particles at large distances after driving, $g_2 < 0$, in contrast, tends to weaken repulsive U even at large $U = 2$ where $\bar{g}(j)$ reaches its maximal value around $j \sim 4$, which is in contrast to $j \sim 8$ in the ground state.

In Fig. 9e) we present average distance \bar{d} in the ground state for two $g_2 = \pm 0.12$ as well as after driving. For $g_2 = -0.12$ the result clearly shows substantially diminished \bar{d} in comparison to its value in the ground state. We now focus to results obtained using $g_2 = 0.12$. By comparing Figs. 9c) and d) we see a clear redistribution of $\bar{g}(j)$ in comparison with $g(j, t = 0)$. The average distance \bar{d} in Figs. 9e) for $g_2 = 0.12$ show a slight increase of \bar{d} after driving for $U < 0.5$ and a

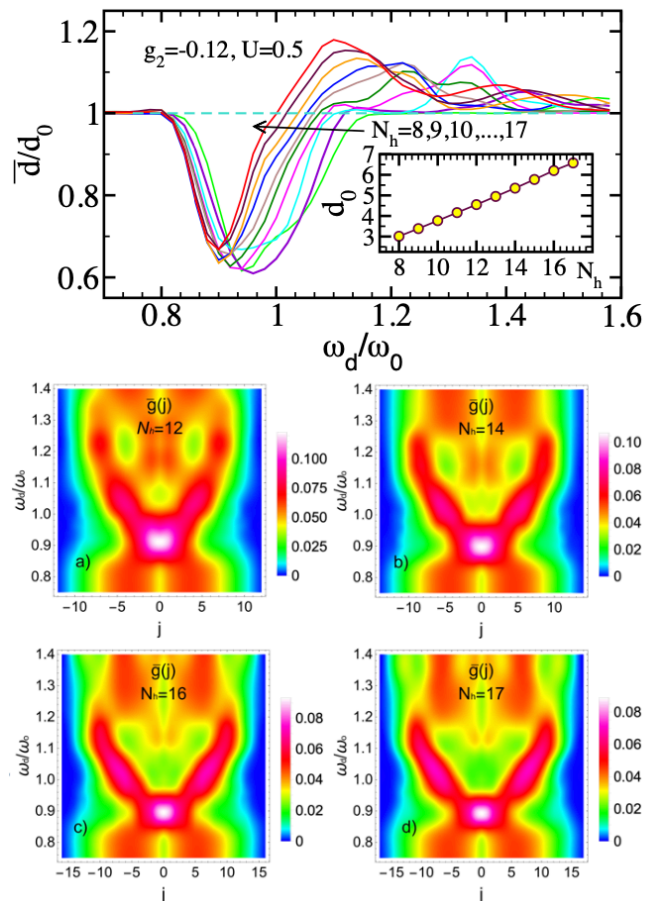


Figure 7: Top figure: the time-averaged \bar{d}/d_0 for different sizes of the Hilbert space ranging from $N_{\text{st}}^{1D} \sim 1600$ for $N_h = 8$, up to $N_{\text{st}}^{1D} \sim 1.1 \times 10^6$ for $N_h = 17$. d_0 represents the average distance in the ground state. Note that N_h represents the maximal number of phonon quanta in the limited Hilbert space. The inset shows the average distance d_0 in the ground state before the pulse has been switched on. The rest of the parameters are identical to those used in Fig. (3) of the main text. From a) through d) we show the evolution of the time-averaged density-density correlation functions $\bar{g}(j)$ with increasing number of basis states generated by $N_h = 12, 14, 16$ and 17 that lead to $N_{\text{st}} = 31064, 130843, 542591$ and 1.1×10^6 basis states, respectively.

slight decrease for $U > 0.5$. Still, changes are too small for results to be conclusive. Note also, that for $g_2 = 0.12$ we have chosen ω_d that seemed optimal to achieve attractive interaction.

VIII. DRIVEN SINGLE-SITE PROBLEM (ANALYTIC SOLUTION)

Numerical simulations show a resonant behavior of the optically driven system. We analyse the driving process analytically in the atomic limit ($t = 0$). The starting point is the

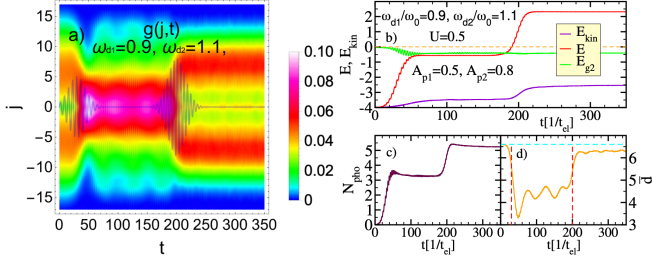


Figure 8: a) $g(j, t)$ in the case of two successive optical pulses with two different ω_d and A_p as denoted in the legend; b) different energies as defined in the caption of Fig. (1) of the main text; c) and d), N_{pho} and \bar{d} , respectively. In d) vertical lines present times $t_1 = 45$ and $t_2 = 200$ of the optical pulses given by $V(t) = A_{p1} \sin(\omega_{d1} t) \exp[-(t - t_1)^2/2\sigma^2] + A_{p2} \sin(\omega_{d2} t) \exp[-(t - t_2)^2/2\sigma^2]$ as also shown with a grey line in a). The other parameters are identical to those used in Fig. (1) of the main text.

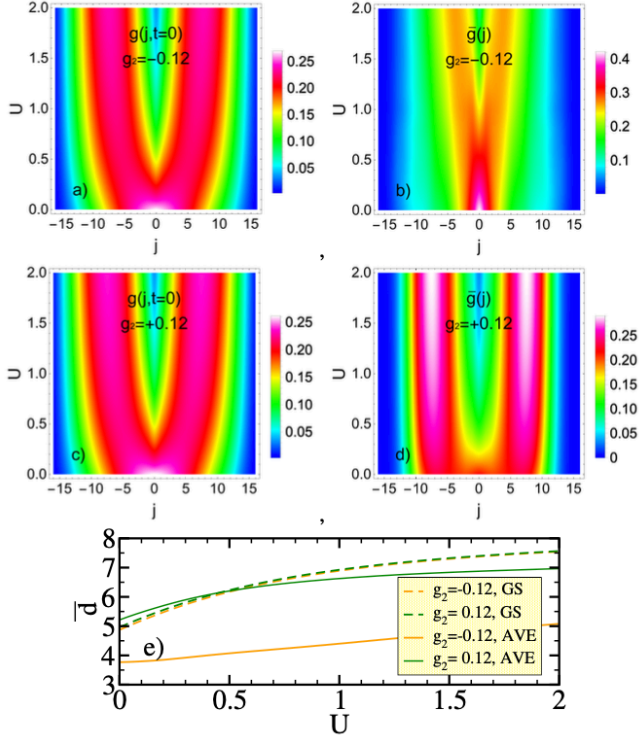


Figure 9: a) and c): the ground-state $g(j, t = 0)$ vs. U for $g_2 = -0.12$ and 0.12 , respectively; b) and d) time-averaged $\bar{g}(j)$ for $g_2 = -0.12$ and 0.12 , respectively. In the latter case, we have used driving frequencies $\omega = 0.9$ and 1.0 , respectively, where maximal attractive interaction is expected based on Figs. 3a) and c) of the main text; e) corresponding average distance \bar{d} , computed in the ground state (GS) and time-averaged after the pulse (AVE). Note that results for $g_2 = \pm 0.12$ in the ground state nearly overlap.

Hamiltonian

$$\mathcal{H}_{at} = U \hat{n}_\uparrow \hat{n}_\downarrow + \omega_0 \left(b^\dagger b + \frac{1}{2} \right) + g_2 \hat{n} \left(b^\dagger + b \right)^2 + F(t) \left(b^\dagger + b \right). \quad (2)$$

First, we apply the squeezing transformation $\tilde{\mathcal{H}}_{at} = e^{\hat{S}_1} \mathcal{H}_{at} e^{-\hat{S}_1}$ proposed by Kennes et al.¹ which rescales the position and momentum of oscillators depending on a local electronic density. The generator of squeezing transformation can be written as

$$\hat{S}_1 = \frac{i}{2} \zeta (\hat{x} \hat{p} + \hat{p} \hat{x}) = -\frac{1}{2} \zeta_j (b^{\dagger 2} - b^2), \quad (3)$$

with the squeezing parameter $\zeta = -\frac{1}{4} \ln \left(1 + \frac{4g_2 \hat{n}}{\omega_0} \right)$.

Bosonic operators are converted into

$$\begin{aligned} b^\dagger &\longrightarrow \tilde{b}^\dagger = b^\dagger \cosh \zeta + b \sinh \zeta \\ b &\longrightarrow \tilde{b} = b \cosh \zeta + b^\dagger \sinh \zeta \end{aligned} \quad (4)$$

while the electron number operator remains unaffected. Hamiltonian takes the following form

$$\tilde{\mathcal{H}}_{at} = U \hat{n}_\uparrow \hat{n}_\downarrow + \omega(\hat{n}) \left(b^\dagger b + \frac{1}{2} \right) + F(t) \left(1 + \frac{4g_2 \hat{n}}{\omega_0} \right)^{-\frac{1}{4}} \left(b^\dagger + b \right), \quad (5)$$

where $\omega(\hat{n}) = \omega_0 \sqrt{1 + \frac{4g_2 \hat{n}}{\omega_0}}$ denotes the electron-density dependent oscillator frequency.

Since $\tilde{\mathcal{H}}_{at}$ has a similar form as the single-site Holstein-Hubbard Hamiltonian we proceed with a transformation analogous to the Lang-Firsov transformation. Based on the form of the Lang-Firsov transformation generator we construct

$$\hat{S}_2 = \frac{F(t)}{\omega_0} \left(1 + \frac{4g_2 \hat{n}}{\omega_0} \right)^{-\frac{3}{4}} (b^\dagger - b). \quad (6)$$

This transformation maps bosonic operators

$$\begin{aligned} b^\dagger &\longrightarrow b^\dagger - \frac{F(t)}{\omega_0} \left(1 + \frac{4g_2 \hat{n}}{\omega_0} \right)^{-\frac{3}{4}} \\ b &\longrightarrow b - \frac{F(t)}{\omega_0} \left(1 + \frac{4g_2 \hat{n}}{\omega_0} \right)^{-\frac{3}{4}} \end{aligned} \quad (7)$$

and yields transformed Hamiltonian of the form

$$\mathcal{H}'_{at} = U \hat{n}_\uparrow \hat{n}_\downarrow + \omega(\hat{n}) \left(b^\dagger b + \frac{1}{2} \right) - \frac{F(t)^2}{\omega_0} \left(1 + \frac{4g_2 \hat{n}}{\omega_0} \right)^{-1}. \quad (8)$$

The electron number operator is once again unaffected by the transformation.

The dependence of the driving response should be reflected in the effective electron-electron interaction which we introduce following Kennes et al.¹ as

$$U_{eff} = (E_2 - E_0) - 2(E_1 - E_0) = E_2 - 2E_1 + E_0, \quad (9)$$

Considering $\tilde{\mathcal{H}}_{at}$ (we find it more convenient to obtain time-dependencies using $\tilde{\mathcal{H}}_{at}$ instead of \mathcal{H}'_{at}) the effective Coulomb interaction takes the following form

$$\begin{aligned}
U_{eff} = & U + \omega(2)\langle b^\dagger b \rangle_2 + \omega_0\langle b^\dagger b \rangle_0 - 2\omega(1)\langle b^\dagger b \rangle_1 \\
& + \frac{1}{2} \left[\omega(2) + \omega_0 - 2\omega(1) \right] + F(t) \left[\gamma(2)\langle b^\dagger + b \rangle_2 \right. \\
& \left. + \langle b^\dagger + b \rangle_0 - 2\gamma(1)\langle b^\dagger + b \rangle_1 \right], \tag{10}
\end{aligned}$$

where $\langle b^\dagger b \rangle_n$ and $\langle b^\dagger + b \rangle_n$ denote the expectation value of the $b^\dagger b$ and $b^\dagger + b$ operators in the propagated state with $n \in \{0, 1, 2\}$ being the electron occupation number. We introduced $\gamma(\hat{n}) = \left(1 + \frac{4g_2\hat{n}}{\omega_0}\right)^{-\frac{1}{4}}$ to obtain expression in a more compact form. The electron occupation number operators in $\omega(\hat{n})$ and $\gamma(\hat{n})$ can be replaced with scalars in the atomic limit.

We believe that there is a strong correlation between the behavior of U_{eff} and the expectation number of phonons excited during the driving. Bearing in mind the mapping of bosonic operators (4) the phonon number operator is written as

$$\begin{aligned}
\hat{N}_{ph}(t) = & b^\dagger(t)b(t) \left(\cosh^2 \zeta(n) + \sinh^2 \zeta(n) \right) + \sinh^2 \zeta(n) \\
& + \left(b^\dagger(t)^2 + b(t)^2 \right) \sinh \zeta(n) \cosh \zeta(n) \tag{11}
\end{aligned}$$

We calculate time evolutions of U_{eff} and $\langle \hat{N}_{ph} \rangle_n$ using the Heisenberg picture. For simplicity we assume the harmonic driving $F(t) = F_0 \sin(\omega_d t)$. The Heisenberg equations of motion with respect to (5) yield

$$\begin{aligned}
b(t) = & b e^{-i\omega(n)t} - \frac{iF_0\gamma(n)\omega_d}{\omega(n)^2 - \omega_d^2} \cos(\omega_d t) \\
& - \frac{F_0\gamma(n)\omega_d}{\omega(n)^2 - \omega_d^2} \sin(\omega_d t), \\
b^\dagger(t) = & b^\dagger e^{i\omega(n)t} + \frac{iF_0\gamma(n)\omega_d}{\omega(n)^2 - \omega_d^2} \cos(\omega_d t) \\
& - \frac{F_0\gamma(n)\omega_d}{\omega(n)^2 - \omega_d^2} \sin(\omega_d t), \tag{12}
\end{aligned}$$

The initial state of the system is a coherent state $|\alpha\rangle$ with $\langle \hat{x}(t=0) \rangle = 0$ and $\langle \hat{p}(t=0) \rangle = 0$. Hence $\Re(\alpha) = 0$ and $\Im(\alpha) = \frac{F_0\gamma(n)\omega_d}{\omega(n)^2 - \omega_d^2}$, where α denotes the eigenvalue of b .

It follows

$$\begin{aligned}
\langle b^\dagger(t)b(t) \rangle_n = & \frac{2F_0^2\gamma(n)^2\omega_d^2}{(\omega(n)^2 - \omega_d^2)^2} \left[1 - \cos(\omega_d t) \cos(\omega(n)t) \right. \\
& \left. - \sin(\omega_d t) \sin(\omega(n)t) \right], \\
\langle b^\dagger(t) + b(t) \rangle_n = & \frac{2F_0\gamma(n)\omega_d}{\omega(n)^2 - \omega_d^2} \left[\sin(\omega(n)t) - \sin(\omega_d t) \right], \\
\langle b^\dagger(t)^2 + b(t)^2 \rangle_n = & \frac{2F_0^2\gamma(n)^2\omega_d^2}{(\omega(n)^2 - \omega_d^2)^2} \left[\sin^2(\omega_d t) - \cos^2(\omega_d t) \right. \\
& \left. - \cos(2\omega(n)t) + 2\cos(\omega_d t) \cos(\omega(n)t) \right. \\
& \left. - 2\sin(\omega_d t) \sin(\omega(n)t) \right], \tag{13}
\end{aligned}$$

which determines the time-evolution of $\langle \hat{N}_{ph} \rangle_n$ and U_{eff} .

In Fig. 10 we plot the time-averaged number of phonons along with the time-averaged potential. We have computed $\langle b^\dagger(t)b(t) \rangle_n$, $\langle b^\dagger(t) + b(t) \rangle_n$ and $\langle b^\dagger(t)^2 + b(t)^2 \rangle_n$ for each $n = 0, 1, 2$ as a function of the driving frequency ω_d . These values determine the ω_d -dependence of $\langle \hat{N}_{ph} \rangle_n$ and U_{eff} . We observe a resonant behavior at frequencies that differ from bare molecular oscillator frequency depending on the electron occupation number and the value of the electron-phonon coupling parameter. At frequencies close to ω_0 and $\omega(2)$ effective Coulomb interaction increases, however, there is also a strong dip in U_{eff} centered at $\omega(1)$.

The most important contribution to U_{eff} comes from $\langle b^\dagger b \rangle_n$. This term would persist even if the driving stops and has the same resonant behavior as the number of phonons that get excited during the driving process.

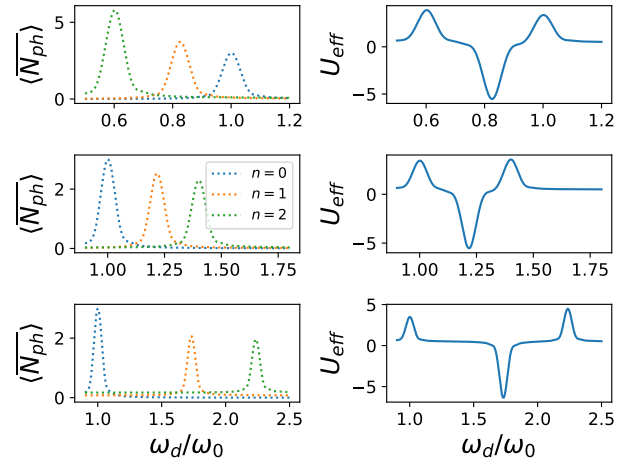


Figure 10: Time-averaged number of phonons and effective potential as a function of the driving frequency. Each row corresponds to a different value of g_2 . The upper one to $g_2 = -0.08$, the middle one to $g_2 = 0.12$ and the bottom one to $g_2 = 0.5$.

IX. PHYSICAL REALIZATIONS OF QUADRATIC COUPLING

In this section, we gather different physical realization where quadratic electron-lattice coupling is dominant.

The first example includes materials with dipolar active phonons in a centrosymmetric system where the linear term is forbidden by symmetry. This is the experimentally relevant example in $\text{K}_3\text{C}_{60}^2$ or $\kappa\text{-(ET)}_2\text{Cu}[\text{N}(\text{CN})_2]\text{Br}$ ($\kappa\text{-Br}$)³.

The second example includes systems formed by a chain of molecular oscillators, each made up of three atoms, with light atoms depicted as yellow spheres and positioned between the heavy ones represented as blue spheres, in Fig. 11(a). As an initial approximation, the motion of the heavy atoms can be neglected, while vibrations of the light atoms are described by independent harmonic oscillators with frequency ω_0 corresponding to optical phonons. As these systems are low-dimensional, we can reduce the heating by using polarization which is perpendicular to the active dimension of the system. While details of the electron-lattice coupling depend on the actual material, we can consider two main contributions: Coulomb interaction between heavy and light nuclei and tunneling terms.

Our approach closely follows derivation given in Ref.⁴ (Ref. ³⁵ in the main manuscript). The first contribution stems from an additional Coulomb interaction between the heavy and light ions due to the presence of the carrier, altering the total charge of the light ion. If we set $U(x)$ as the supplementary Coulomb interaction induced by the carrier, the potential increases by $U(d + \delta x) + U(d - \delta x)$, where d denotes the equilibrium distance between the light and heavy ions, see Fig. 11. This function is even with respect to δx , implying an absence of linear or odd terms in δx . Consequently, the interaction component of the Hamiltonian can be expressed as $\mathcal{H}_{int} \propto \sum_j n_j \delta x_j^2 \propto \sum_j n_j (a_j^\dagger + a_j)^2$, where a_j^\dagger (a_j) represents an operator that creates (annihilates) a phonon on the j -th harmonic oscillator, and n_j signifies the electron density operator of the j -th site.

The second mechanism, termed hybridization, explains the EP coupling term in the Hamiltonian as a result of virtual hopping processes within the second-order perturbation theory. The overlap of orbitals of light and heavy ions is represented by the hopping integral $t'(x)$, depending on the distance between the ions. The carrier can decrease its on-site energy by $-t'^2/\Delta$ via virtual hopping to a neighboring heavy ion and back. Here, Δ represents the energy difference between the carrier residing in the light ion's orbital and an electron occupying the heavy ion's orbital. We assume Δ to be substantial, resulting in a negligible probability of the carrier occupying the heavy ion. In instances of small δx , the hopping can be approximated to the lowest order as $t_0(1 + \alpha\delta x)$, where $t_0 = t'(x = d)$, and α represents a material-specific constant. Two contributions emerge from the carrier's ability to hop to either of the two heavy ions, amounting to

$$\frac{-t_0^2}{\Delta} [(1 + \alpha\delta x)^2 + (1 - \alpha\delta x)^2] = \frac{-2t_0^2}{\Delta} [1 + \alpha^2\delta x^2] \quad (14)$$

Given that the change in energy manifests as a quadratic func-

tion of δx , it follows that $\mathcal{H}_{int} \propto \sum_j \hat{n}_j (a_j^\dagger + a_j)^2$ and importantly the prefactor of such contribution is negative relevant for photo-induced pairing introduced in the main text.

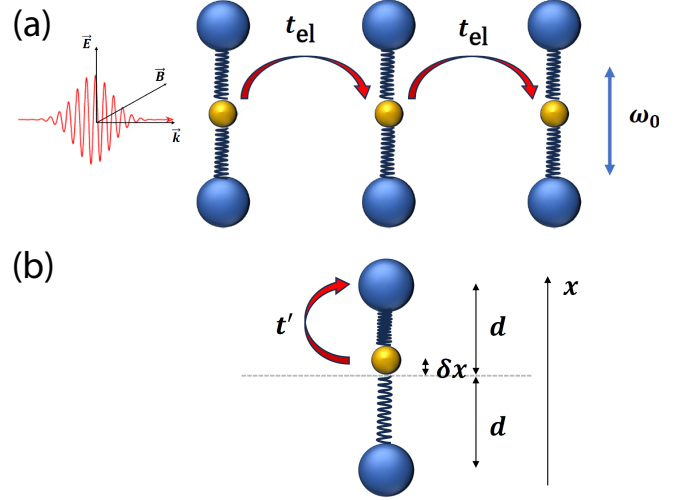


Figure 11: a) Sketch of a setup with a low-dimensional system where light ions are symmetrically intercalated between heavy ions and the electric field whose polarization is applied perpendicular to the direction of the lattice. b) Sketch of the displacement.

-
- ¹ D. M. Kennes, E. Y. Wilner, D. R. Reichman, and A. J. Millis, *Nature Physics* **13**, 479 (2017), URL <https://doi.org/10.1038/nphys4024>.
- ² M. Mitrano, A. Cantaluppi, D. Nicoletti, S. Kaiser, A. Perucchi, S. Lupi, P. Di Pietro, D. Pontiroli, M. Riccò, S. R. Clark, et al., *Nature* **530**, 461 (2016), URL <https://doi.org/10.1038/nature16522>.
- ³ M. Buzzi, D. Nicoletti, M. Fechner, N. Tancogne-Dejean, M. A. Sentef, A. Georges, T. Biesner, E. Uykur, M. Dressel, A. Henderson, et al., *Phys. Rev. X* **10**, 031028 (2020), URL <https://link.aps.org/doi/10.1103/PhysRevX.10.031028>.
- ⁴ C. P. J. Adolphs and M. Berciu, *Phys. Rev. B* **89**, 035122 (2014), URL <https://link.aps.org/doi/10.1103/PhysRevB.89.035122>.